Progress In Electromagnetics Research, PIER 76, 253–274, 2007

BISTATIC SCATTERING FROM ROUGH DIELECTRIC SOIL SURFACE WITH A CONDUCTING OBJECT WITH ARBITRARY CLOSED CONTOUR PARTIALLY BURIED BY USING THE FBM/SAA METHOD

Z.-X. Li

Electromagnetic Academy
Zhejiang University
Hangzhou, Zhejiang, China, 310075

Abstract—A hybrid approach of the forward-backward method (FBM) with spectral accelerate algorithm (SAA) and Monte Carlo method is developed in this paper. It is applied to numerical simulation of bistatic scattering from one-dimensional arbitrary dielectric constant soil surface with a conducting object with arbitrary closed contour partially buried under both the horizontal and vertical polarization tapered wave incidence at low grazing angle. The energy conservation has been checked for the FBM/SAA. Numerical simulations of bistatic scattering at low grazing angle have been discussed in this paper.

1. INTRODUCTION

A novel and powerful iterative numerical technique called FBM has been proposed by Holliday et al. [1] for solving the magnetic field integral equation (MFIE) recent year, which describes the induced currents along one-dimensional (1-D) perfect electrically conducting (PEC) rough surface. A similar approach called the method of ordered multiple interactions (MOMI) has been simultaneously proposed by Kapp and Brown [2]. The method has shown a very fast convergence, obtained accurate results within very few iterations, which makes them computationally effective. The operational counts is $O(N^2)$ (of order N^2) and, thus, the simulation of quite large surfaces becomes possible, even for low grazing angle (LGA) incidence. The FBM for PEC rough surface has been accelerated by novel SAA first described in [3], and then implemented for both MFIE and electric field integral equation (EFIE) in [4]. The computational cost and storage requirements are further reduced to $O(N)$.

In [5] and [6], the FBM has been extended to the case of 1-D imperfect conducting rough surface with a high imaginary part of the complex dielectric constant, such as sea surface at microwave frequencies. And SAA is used to accelerated the FBM in [6]. The computational cost and storage requirements are also reduced to $O(N)$. Meanwhile, the FBM has been developed to simulatively calculate the RCS of large open-ended cavities by combined with physical optics algorithm [7, 8].

The FBM has been further developed to calculate the scattering from 1-D dielectric rough surface with arbitrary dielectric constant in [9–12]. To speed up the FBM calculation, the SAA of Green's function was proposed and implemented in [9] and [10], so the computational cost and storage requirements of the FBM/SAA are also reduced to $O(N)$.

Electromagnetic scattering from the arbitrary shape target above, on (partially buried) and below a rough surface has attracted much interest during recent year [15–20]. So the FBM/SAA remains to be required to be further improved for solving of scattering from inhomogeneous composite rough surface with large arbitrarily shaped conducting object partially buried, as described in Fig. 1.

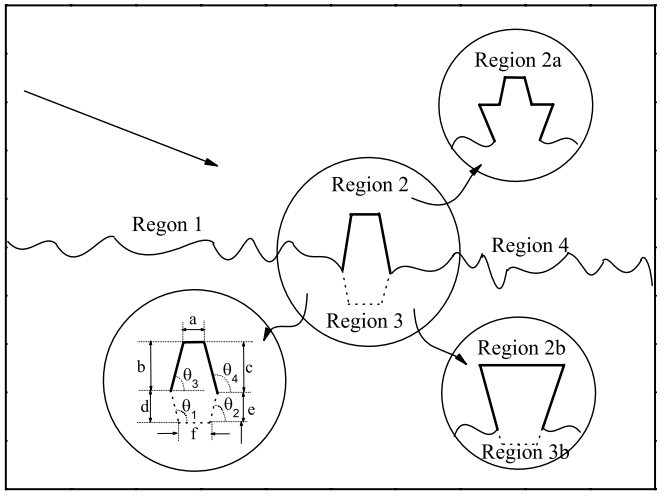

Figure 1. Rough dielectric soil surface and partially buried conducting SSPO.

To calculate scattering from 1-D spatially inhomogeneous composite dielectric rough surface with large arbitrarily shaped conducting object partially buried, we should study the characteristic of the closed contour curve of the arbitrarily shaped conducting object

above the rough surface. The closed contour curve can be separated into two parts, one is above the rough surface (see Region 2 in Fig. 1), another one is below the rough surface (see Region 3 in Fig. 1). If we consider the dielectric rough sea surface as PEC rough surface at microwave frequencies, which is good approximation for problem of wave scattering from sea surface at high frequency, then we can just study the curve above the rough surface. If the curve is a multi-value function of x, for example, ship target on the sea surface (see Region 2a in Fig. 1), the aforementioned conventional FBM is not well tractable to have good convergence to the problem, but a new approach general FBM (GFBM) has been recently developed in [13], [21] and [22] to calculate scattering from the kind of composite rough surface consisting of a conducting ship target above PEC rough sea surface. The GFBM combines the conventional FBM with the Method of Moment (MoM), where the MoM is only applied to the region of the obstacle. Meanwhile, SAA has used to accelerate the GFBM, which was first described in [13] and [14], and was also implemented in [21] and [22]. The GFBM/SAA has been further achieved to calculate scattering from 1-D impedance rough sea surface with a conducting ship present at both horizontal and vertical polarization incident wave cases (call TE case and TM case later, respectively) at LGA [23]. The GFBM/SAA asks for a high imaginary part of the complex dielectric constant to satisfy the impedance boundary condition. It should be pointed out that all the aforementioned GFBM/SAA [13, 14, 21–23] haven't been used to calculate the kind of composite rough surface scattering problem, which is the rough surface with a closed contour of conducting object partially buried.

If we want to study the scattering from the dielectric rough surface with arbitrary dielectric constant and with a arbitrary shaped conducting object partially buried, we should study the characteristic of both two parts of contour curve of the arbitrary shaped conducting object above and below the rough surface. If the part of contour curve of the arbitrary shaped conducting object above the rough surface is multi-value function of abscissa x(see Region 2b and 3b in Fig. 1), the GFBM/SAA has been achieved to calculate the kind of composite rough surface problem [26]. If both two parts are only single-value function of abscissa x rather then multi-value function of x, for example, a conducting Six-Side Polygon Object (SSPO) (see Region 2 and 3 in Fig. 1), the aforementioned FBM(/SAA) [1–12] can't be simple used to solve the kind of composite rough surface problem, although the FBM (or equivalent MOMI) can be used to calculate scattering from closed contour of conducting object, for examples, 2-dimensional infinite elliptical cylinders ([24] and [25]). So the FBM/SAA need be

further developed by introduced new calculation technique to solve this kind of inhomogeneous composite rough surface problem.

In this paper, based upon above advance of the FBM, GFBM and other studies of LGA problems, a hybrid method of the FBM with the SAA is developed. It is applied to numerically simulation of bistatic scattering from 1-D arbitrary dielectric constant rough soil surface with a conducting SSPO partially buried under the TE or TM tapered wave incidence at LGA. The transmitting fields have been calculated in this approach to check the energy conservation.

The paper is organized as follow. In Section 2.1, EFIE and MFIE of the dielectric and conducing rough surfaces are introduced. In Section 2.2, FBM/SAA for dielectric and PEC rough surface is reviewed. In Section 2.3, FBM/SAA for dielectric rough soil surface with a conducting SSPO partially buried is introduced. In Section 3, numerical results are analyzed. Finally, conclusion is given in Section 4.

2. METHODOLOGY

2.1. EFIE and MFIE

We are concerned with a tapered plane wave $E^{in}(x,z)$ $H^{in}(x,z)$ with horizontal polarization (TE) or vertical polarization(TM), incident upon a 1-D dielectric rough surface. Random surface height has $z = f(x)$ and $< f(x) >= 0$. The coupled surface integral equations are written as [27]

$$V(r) = \frac{X_0(r)}{2} - \int_{S'} \left\{ X_0(r') \frac{\partial g(r,r')}{\partial n'} - g(r,r') \frac{\partial X_0(r')}{\partial n'} \right\} dS' \quad (1)$$

$$0 = \frac{X_1(r)}{2} + \int_{S'} \left\{ X_1(r') \frac{\partial g_1(r,r')}{\partial n'} - g_1(r,r') \frac{\partial X_1(r')}{\partial n'} \right\} dS' \quad (2)$$

where for TE case: $X_0(r) = E_0(r)$, $V(r) = E^{in}(r)$; for TM case: $X_0(r) = H_0(r)$, $V(r) = H^{in}(r)$. The boundary conditions are written as $X_1(r) = X_0(r)$ and $\frac{\partial X_1(r)}{\partial n'} = \rho \frac{\partial X_0(r)}{\partial n'}$, $\rho = 1$, for TE case, $\rho = \frac{\varepsilon_1}{\varepsilon_0}$, for TM case. Here r is at the surface. The $g(r,r')$, $g_1(r,r')$, $\frac{\partial g(r,r')}{\partial n'}$ and $\frac{\partial g_1(r,r')}{\partial n'}$ are, respectively, the 2-D above-space and below-space Green's function and its normal derivative: $g(r,r') = \frac{i}{4} H_0^1(k_0|r-r'|)$, $g_1(r,r') = \frac{i}{4} H_0^{(1)}(k_1|r-r'|)$, where $H_0^{(1)}(\bullet)$ is the first kind Hankel function with zeroth order.

For PEC rough surface, E_0, E_1 and $\frac{\partial E_1}{\partial n'}$ will be zero for TE case, and $\frac{\partial H_0}{\partial n'}$, H_1 and $\frac{\partial H_1}{\partial n'}$ will be zero for TM case.

2.2. FBM/SAA for Rough Surface

2.2.1. FBM

The integral equation is then discretized using an evenly spaced single grid. The dielectric rough surface is discretized into a single grid of N points for x between $-L/2$ and $L/2$ (L is the surface length illuminated by tapered wave), and the points x_m is written as $x_m = (m-0.5)\Delta x$, $m = 1, 2, ..., N$. So, applying rectangular pulse basis function and point match method of MoM [28], the Eqs. (1) and (2) become

$$\begin{bmatrix} \overline{\overline{Z}}_a & \overline{\overline{Z}}_b \\ \overline{\overline{Z}}_c & \overline{\overline{Z}}_d \end{bmatrix} \cdot \begin{bmatrix} \overline{X}_1 \\ \overline{X}_2 \end{bmatrix} = \begin{bmatrix} \overline{V} \\ 0 \end{bmatrix} \tag{3}$$

where X_1 is called induced magnetic current and X_2 is called induced electrical current later. For TE case: $X_1 = E_0$, $X_2 = \sqrt{1+f_x^2}\frac{\partial E_0}{\partial n'}$, $V = E^{in}$. For TM case: $X_1 = H_0$, $X_2 = \sqrt{1+f_x^2}\frac{\partial H_0}{\partial n'}$, $V = H^{in}$. The matrix elements $\overline{\overline{Z}}_a$, $\overline{\overline{Z}}_b$, $\overline{\overline{Z}}_c$ and $\overline{\overline{Z}}_d$ are given by [9] or [10].

It is desirable to make the following decomposition: $\overline{X}_j = \overline{X}_{jf} + \overline{X}_{jb}$ $(j = 1, 2)$, $\overline{\overline{Z}}_l = \overline{\overline{Z}}_l^f + \overline{\overline{Z}}_l^s + \overline{\overline{Z}}_l^b$ $(l = a, b, c, d)$, where $\overline{X}_{jf}$ $(j = 1, 2)$, are the forward components (i.e., the induced magnetic $(j = 1)$ or induced electric $(j = 2)$ current contribution due to the waves propagating in the forward direction), $\overline{X}_{jb}$ $(j = 1, 2)$, are the backward components (i.e. the induced magnetic $(j = 1)$ or induced electric $(j = 2)$ current contribution due to the waves propagating in the backward direction). $\overline{\overline{Z}}_l^f$, $\overline{\overline{Z}}_l^s$ and $\overline{\overline{Z}}_l^b$ $(l = a, b, c, d)$ of Eqs. (3) are, respectively, the lower triangular part, the diagonal part (self impedance terms), and the upper triangular part of $\overline{\overline{Z}}_l$ in Eq. (3).

After matrices and vectors of Eq. (3) are separated, an iterative solution can be gotten [9–12], and the unknowns in the *jth* iteration $(\overline{X}_{1f}^{(j)}, \overline{X}_{2f}^{(j)}, \overline{X}_{1b}^{(j)}, \overline{X}_{2b}^{(j)})$ can be written in unified form

$$(\overline{\overline{Z}}_p^s + \overline{\overline{Z}}_p^f)\overline{X}_{1f}^{(j)} + (\overline{\overline{Z}}_q^s + \overline{\overline{Z}}_q^f)\overline{X}_{2f}^{(j)} = \overline{V} - \overline{\overline{Z}}_p^f\overline{X}_{1b}^{(j-1)} - \overline{\overline{Z}}_q^f\overline{X}_{2b}^{(j-1)} \tag{4}$$

$$(\overline{\overline{Z}}_p^s + \overline{\overline{Z}}_p^b)\overline{X}_{1b}^{(j)} + (\overline{\overline{Z}}_q^s + \overline{\overline{Z}}_q^b)\overline{X}_{2b}^{(j)} = -\overline{\overline{Z}}_p^b\overline{X}_{1f}^{(j)} - \overline{\overline{Z}}_q^b\overline{X}_{2f}^{(j)} \tag{5}$$

where (1) integral equation for above space: $V = E^{in}(r)$ for TE case and $V = H^{in}(r)$ for TM case, $p = a$, $q = b$; (2) integral equation for below space: $V = 0$ for both TE and TM case, $p = c$, $q = d$.

The algorithm starts with $\overline{X}_{1b}^{(0)} = 0$ and $\overline{X}_{2b}^{(0)} = 0$. The detailed algorithm has been given in [9–12]. It converges extremely fast for moderately rough surfaces (less than six iterations).

For PEC surface, $Z_a = Z_c = Z_d = 0$ and $X_1 = 0$ for TE case; $Z_b = Z_c = Z_d = 0$ and $X_2 = 0$ for TM case in the Eq. (3). Meanwhile, $X_1 = 0$ and $X_2 = 0$ for TE and TM case, respectively, in Eqs. (4) and (5). The detailed algorithm can referred to [1, 2, 4]. it converges extremely fast for moderately rough surfaces, e.g., less than six iterations.

2.2.2. The SAA of Green's Function

From Eqs. (4) and (5), we know that the forward-backward iterative procedure described above requires repeated computation of the matrix-vector products, such as $\overline{\overline{Z}}_l^f \cdot \overline{X_1}$, $\overline{\overline{Z}}_l^f \cdot \overline{X_2}$, $\overline{\overline{Z}}_l^b \cdot \overline{X_1}$ and $\overline{\overline{Z}}_l^b \cdot \overline{X_2}$, $(l = a, b, c, d)$, i.e., which can be written in unified form

$$U_f^{(j)}(r_n) = \sum_{m=1}^{n-1} Z_{mn}^{(p)} X_{1m} + \sum_{m=1}^{n-1} Z_{mn}^{(q)} X_{2m} \tag{6}$$

$$U_b^{(j)}(r_n) = \sum_{m=n+1}^{N} Z_{mn}^{(p)} X_{1m} + \sum_{m=n+1}^{N} Z_{mn}^{(q)} X_{2m} \tag{7}$$

where $n = 1, 2, ..., N$. The functions of $U_f^{(j)}$ and $U_b^{(j)} (j = 1, 2)$, denote the forward (f) and backward (b) radiation by the source current elements in the upper media $(j = 1)$ and lower media $(j = 2)$ of the receiving nth element, respectively. Meanwhile, for $j = 1$ case: $p = a$, $q = b$; for $j = 2$ case: $p = c$, $q = d$. Calculation in per iteration takes $O(N^2)$ operations. When the SAA is applied to Eqs. (6)–(7), the operational count and memory storage can be reduced to $O(N)$.

Let's choose a neighborhood distance L_s. Interactions between the points within L_s are classified as strong and those outside of L_s as weak (seen Fig. 2). For example, Eq. (6) can be written as

$$\begin{aligned} U_f^{(j)}(r_n) &= U_s^{(j)}(r_n) + U_w^{(j)}(r_n) \\ &= \sum_{m=n-N_s-1}^{n-1} (Z_{mn}^{(p)} X_{1m} + Z_{mn}^{(q)} X_{2m}) \\ &\quad + \sum_{m=1}^{n-N_s-1} (Z_{mn}^{(p)} X_{1m} + Z_{mn}^{(q)} X_{2m}) \end{aligned} \tag{8}$$

where $p = a$, $q = b$ for $j = 1$; $p = c$, $q = d$ for $j = 2$.

$U_s^{(j)}$ is found in conventional manner using the exact matrix elements. The weak contribution $U_w^{(j)}$ radiated from the source group

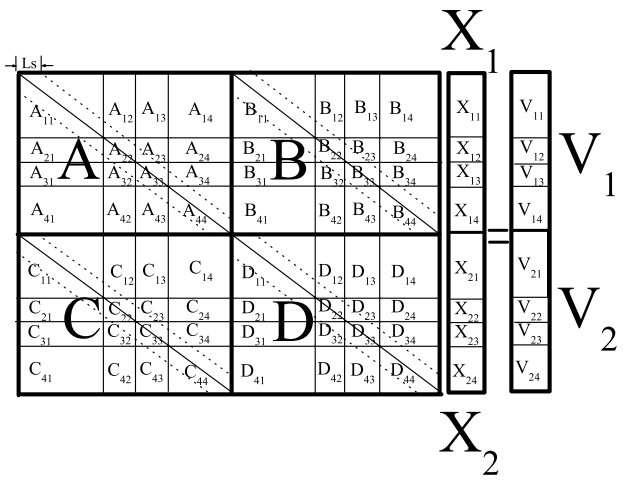

Figure 2. Matrix equations for both TE and TM cases.

outside the strong source group becomes important when the incidence angle approaches to grazing or if one is interested in backscattered field. The computation of $U_w^{(j)}$ can be accelerated via the SAA.

Substituting the spectral representation of Green's function and its normal derivative [6]:

it is derived that

$$\begin{aligned} U_w^{(j)}(r_n) &= \sum_{m=1}^{n-N_s-1} (Z_{nm}^{(p)} X_{1m} + Z_{nm}^{(q)} X_{2m}) \\ &= \frac{i\Delta x}{4\pi} \int_{C_\theta} F_n(\theta) e^{ik_i z_n \sin\theta} d\theta \end{aligned} \tag{9}$$

where

$$\begin{aligned} F_n(\theta) &= F_{n-1}(\theta) e^{ik_i \Delta x \cos\theta} \\ &\quad + [ik_i(-\sin\theta + f_{x_m}\cos\theta) X_{1n-N_s-1} - \rho X_{2n-N_s-1}] \\ &\quad \times e^{ik_i(N_s+1)\Delta x \cos\theta} e^{-ik_i z_{n-N_s-1}\sin\theta} \end{aligned} \tag{10}$$

where for $j = 1$ case: $p = a$, $q = b$, $k_i = k_0$ and $\rho = 1$; for $j = 2$ case: $p = c$, $q = d$, $k_i = k_1$, $\rho = 1$ for TE case and $\rho = \frac{\varepsilon_1}{\varepsilon_0}$ for TM case.

Eq. (7) can be treated to combined with the SAA in the same way as Eq. (6).

For PEC rough surface, $j = 1$, $p = a$ and $X_2 = 0$ for TE case; $j = 1$, $p = b$ and $X_1 = 0$ for TE case in the Eqs. (6) and (7). The

acceleration algorithm for PEC rough surface is just like the SAA for dielectric rough surface for Eq. (6). In Eq. (10) of the SAA for PEC rough surface, $X_{1n-N_s-1} = 0$ for TE case, and $X_{2n-N_s-1} = 0$ for TM case.

It can be seen from Eq. (10) that can be easily obtained by recursive procedure. In practice, it is described to employ a new integration contour C_δ instead of C_θ in Eq. (9). The criterions in selecting in C_δ and implementing for the spectral integral have been well described in [6, 10, 3, 23].

2.3. FBM/SAA for Dielectric Rough Surface with a Conducting SSPO Partially Buried

Since the characteristic of the dielectric rough surface and conducting SSPO must be taken into consideration simultaneous here, so FBM/SAA should be further developed to calculate the scattering from inhomogeneous complex rough surface. Although the contour of SSPO is close, it can be detached from the rough soil surface into two parts, one of which is above the soil surface, another one is below the soil surface, just like shown in Fig. 1. So the complex rough surface has been divided into four parts. Part 1 is dielectric rough soil surface before SSPO (call dielectric rough soil surface I (**DRSSI**) later), which is Region 1 in Fig. 1. Part 2 is conducting SSPO surface above rough soil surface (call conducting SSPO surface I (**CSSPOSI**) later), which is Region 2 in Fig. 1. Part 3 is conducting SSPO surface below rough soil surface (call conducting SSPO surface II (**CSSPOSII**) later), which is Region 3 in Fig. 1. Last part 4 is dielectric rough soil surface behind SSPO (call dielectric rough soil surface II (**DRSSII**) later), which is Region 4 in Fig. 1.

The differences between FBM/SAA for homogeneous and inhomogeneous dielectric soil surface case are complicated. The matrix equations are the discretisation of Eqs. (1) and (2), the integral in the upper equation (Eq. (1)) must now be extended to surface S, which consists of the **DRSSI**, **CSSPOSI** and **DRSSII**, whereas the integral in the lower equation (Eq. (2)) must now be extended to a different surface S, which consists of the **DRSSI**, **CSSPOSII** and **DRSSII**. In this way, we have the matrix equations, which can be shown in Fig. 2 for TE or TM case.

The Fig. 2 shows that the big equations block coefficient matrix has be divided into four small block matrices **A**, **B**, **C** and **D**, right term vector **V** has been divided into two parts $\mathbf{V}_1$ and $\mathbf{V}_2$, unknown vector **X** has also been divided into two parts $\mathbf{X}_1$ and $\mathbf{X}_2$. However, each small block matrix and vector should be further divided into

more small parts while considering the characteristic of inhomogeneous complex rough surface.

For TE case, Fig. 2 shows:

(i) Small block matrix **B** has sixteen small parts, which describes the interactions among induced electric currents along the inhomogeneous complex rough surface in above space. Note that third column and row part ($\mathbf{B}_{13}, \mathbf{B}_{23}, \mathbf{B}_{33}, \mathbf{B}_{43}, \mathbf{B}_{31}, \mathbf{B}_{32}, \mathbf{B}_{34}$) is zero, which describes interactions between induced electric currents along the **CSSPOSII** and the one along complex rough surface above space. The reason why the parts are zero is that because matrix equation is discretisation Eq. (1) along the above complex rough surface consisting of the **DRSSI**, **CSSPOSI** and **DRSSII**. So the small block matrix **B** has nine small parts left now ($\mathbf{B}_{11}, \mathbf{B}_{21}, \mathbf{B}_{41}, \mathbf{B}_{12}, \mathbf{B}_{22}, \mathbf{B}_{42}, \mathbf{B}_{14}, \mathbf{B}_{24}, \mathbf{B}_{44}$). The left column parts ($\mathbf{B}_{11}, \mathbf{B}_{21}, \mathbf{B}_{41}$) describe the interactions between induced electric currents along the **DRSSI** and the one along other two parts (including the **CSSPOSI** and **DRSSII**). The middle column parts ($\mathbf{B}_{12}, \mathbf{B}_{22}, \mathbf{B}_{42}$) describe the interactions between induced electric currents along the **CSSPOSI** and the one along its two side's dielectric soil surfaces. Just like left column parts, the right column parts ($\mathbf{B}_{14}, \mathbf{B}_{24}, \mathbf{B}_{44}$) describe the interactions between induced electric currents along the **DRSSII** and the one along other two parts (including the **CSSPOSI** and dielectric **DRSSI**).

(ii) Small block matrix **D** also has sixteen small parts, and is just similar with small block matrix **B**, which describes the interactions among induced electric currents along the inhomogeneous complex rough surface in below space rather than above space.

(iii) Small block matrix **A** has sixteen small parts, which describes interactions among the induced magnetic currents along inhomogeneous complex surface in above space. Note that second and third column and row parts ($\mathbf{A}_{12}, \mathbf{A}_{13}, \mathbf{A}_{22}, \mathbf{A}_{23}, \mathbf{A}_{32}, \mathbf{A}_{33}, \mathbf{A}_{21}, \mathbf{A}_{31}, \mathbf{A}_{24}, \mathbf{A}_{34}$) are all zero. For TE case, no matter where the parts is located at the **CSSPOSI**, induced magnetic currents along the surface is zero. So small block matrix **A** has four parts left now ($\mathbf{A}_{11}, \mathbf{A}_{41}, \mathbf{A}_{14}, \mathbf{A}_{44}$). The left column parts ($\mathbf{A}_{11}, \mathbf{A}_{41}$) describe the interactions between induced magnetic currents along the **DRSSI** and **DRSSII**. The right column parts ($\mathbf{A}_{14}, \mathbf{A}_{44}$) describe the reversed interactions.

(iv) Small block matrix **C** is similar with small block matrix **A**. The difference between them is small block **C** describes situations of the complex rough surface in below space.

(v) Right term vectors $\mathbf{V}_1$ and $\mathbf{V}_2$ describe the incident TE wave along the inhomogeneous complex rough surface, respectively. Evidently, $\mathbf{V}_2 = 0$, $\mathbf{V}_{11}$ and $\mathbf{V}_{14}$ describe incident TE waves along the **DRSSI** and **DRSSII**. And $\mathbf{V}_{12}$ describe incident TE waves along the **CSSPOSI**. $\mathbf{V}_{13} = 0$, this is because no incident wave along the **CSSPOSII**.

(vi) Unknown vectors $\mathbf{X}_1$ and $\mathbf{X}_2$ describe the induced current along the inhomogeneous complex rough surface in above and below space. $\mathbf{X}_{11}$ and $\mathbf{X}_{14}$ describe induced magnetic currents along the **DRSSI** and **DRSSII**, $\mathbf{X}_{21}$ and $\mathbf{X}_{24}$ describe induced electric currents along the **DRSSI** and **DRSSII**, $\mathbf{X}_{22}$ describe induced electric currents along the **CSSPOSI**, and $\mathbf{X}_{23}$ describes induced electric currents along the **CSSPOSII**. $\mathbf{X}_{12}$ and $\mathbf{X}_{13}$ describes the induced magnetic currents along the **CSSPOSI** and **CSSPOSII**, so $\mathbf{X}_{12} = 0$ and $\mathbf{X}_{13} = 0$ respectively.

Next, for the TM case, we know that the situations for TM case are just like the one for TE case, the differences between two cases are generated from the polarization of incident waves, so the detailed structure of four small matrices ($\mathbf{A}$, $\mathbf{B}$, $\mathbf{C}$ and $\mathbf{D}$) from TM case is reversed from the one from TE case, so do unknown vector $\mathbf{X}$.

A description of the solution procedure can be seen as follows. For $j$the iteration:

(a) forward propagation procession

(i) Find $X_{11f}^{(j)}$ and $X_{21f}^{(j)}$ over Region 1 using the forward propagation principle; like FBM/SAA for dielectric rough surface, the FBM/SAA is used to solve the four small matrices $(\mathbf{A}_{11}, \mathbf{B}_{11}, \mathbf{C}_{11}, \mathbf{D}_{11})$ to get the forward components of induced currents along the **DRSSI**.

(ii) Find $X_{12f}^{(j)}$ (for TM case) or $X_{22f}^{(j)}$ (for TE case) over Region 2 using the fields radiated by the induced currents along Region 1 plus the incident fields as excitation; just like FBM/SAA for PEC rough surface, the FBM/SAA is used to calculate the forward components of induced currents along the **CSSPOSI** through small matrix $\mathbf{B}_{22}$ (for TE case) or $\mathbf{A}_{22}$ (for TM case).

(iii) Find $X_{13f}^{(j)}$ (for TM case) or $X_{23f}^{(j)}$ (for TE case) over Region 3 by the forward propagation principle; just like FBM/SAA for PEC rough surface, the FBM/SAA is used to calculate the forward components of induced currents along the **CSSPOSII** through small matrix $\mathbf{D}_{33}$ for (TE case) or $\mathbf{C}_{33}$ (for TM case).

(iv) Find $X_{14f}^{(j)}$ and $X_{24f}^{(j)}$ over Region 4 by the forward propagation principle; after the forward components of induced currents

along **CSSPOSI** and **DRSSI** has calculated, FBM/SAA for dielectric rough surface is used to calculate forward components of induced currents along the **DRSSII** through four small matrices $(\mathbf{A}_{44}, \mathbf{B}_{44}, \mathbf{C}_{44}, \mathbf{D}_{44})$.

(b) backward propagation procession

(i) Find $X_{14b}^{(j)}$ and $X_{24b}^{(j)}$ over Region 4 by the backward propagation principle; like FBM/SAA for dielectric rough surface, the FBM/SAA is used to solve the four small matrices $(\mathbf{A}_{44}, \mathbf{B}_{44}, \mathbf{C}_{44}, \mathbf{D}_{44})$ to get backward components of induced currents along the **DRSSII**.

(ii) Find $X_{13b}^{(j)}$ (for TM case) or $X_{23b}^{(j)}$ (for TE case) over Region 3 by the backward propagation principle; just like FBM/SAA for PEC rough surface, the FBM/SAA is used to calculate the backward components of induced currents along the **CSSPOSII** through small matrix $\mathbf{D}_{33}$ (for TE case) or $\mathbf{C}_{33}$ (for TM case).

(iii) Find $X_{12b}^{(j)}$ (for TM case) or $X_{22b}^{(j)}$ (for TE case) over Region 2 using the fields radiated by the backscattering components of induced currents along Region 4; just also like FBM/SAA for PEC rough surface, the FBM/SAA is also used to calculate the backward components of induced currents along the **CSSPOSI** through small matrix $\mathbf{B}_{22}$ (for TE case) or $\mathbf{A}_{22}$ (for TM case).

(iv) Find $X_{11b}^{(j)}$ and $X_{21b}^{(j)}$ over Region 1 using the backward propagation principle, after the backward components of induced currents along the **CSSPOSI** and **DRSSII** has been calculated, FBM/SAA for dielectric rough surface is used to calculate the backward components of induced currents along the **DRSSI** through four small matrices $(\mathbf{A}_{11}, \mathbf{B}_{11}, \mathbf{C}_{11}, \mathbf{D}_{11})$.

(c) the forward-backward propagation procession will repeat till arrive at set error. The algorithm will not exhibit convergent behavior for extremely rough surface, and convergence of the algorithm is extremely fast for moderately rough surfaces, e.g., less than ten iterations.

Computational cost of the FBM/SAA for inhomogeneous dielectric rough surface is practically the same as the conventional FBM/SAA for homogeneous dielectric rough surface.

3. NUMERICAL RESULTS AND DISCUSS

It is worth noting that natural soil surface are usually neither exponentially nor Gaussian correlated, but show intermediate

properties between these two models, and can be better described by using power law spectra and fractal geometry conception [29, 30]. The fractal surface is described by the band-limited Weierstrass-Manderbrot function as

$$f(x) = \delta \cdot C\Sigma_{m=0}^{M-1} b^{(D-2)m} \sin(K_0 b^m x + \varphi_m) \tag{11}$$

where $D(1 < D < 2)$ is fractal dimension, φ_m is random phase, $b(> 1)$ spatial frequency scaling parameter, K_0 the fundamental spatial wave number, and δ is rms surface height, M is the highest number of spatial wave, $C = \sqrt{\frac{2(1-b^{2(D-2)})}{(1-b^{2M(D-2)})}}$ is a normalized amplifier parameter [31]. According to *in situ* measurements [32] and [33], the fractal dimension D of natural soil surface profiles is usually smaller than about 1.5.

The frequency is set equal to 1 GHz, so wavelength of incident tapered wave is 0.3 m, and the tapered parameter of the incident wave w is taken as $16.8\,\mathrm{m} = 56\lambda$, the length of soil surface is $94.8\,\mathrm{m} = 316\lambda$, the geometric size of the conducting SSPO is given as: $a = 1\,\mathrm{m} = 3.33\lambda$, $b = 1\,\mathrm{m} = 3.33\lambda$, $c = 1\,\mathrm{m} = 3.33\lambda$, $d = 1\,\mathrm{m} = 3.33\lambda$, $e = 1\,\mathrm{m} = 3.33\lambda$, $\theta_1 = 100^\circ$, $\theta_2 = 80^\circ$, $\theta_3 = 100^\circ$ and $\theta_4 = 80^\circ$ as described in Fig. 1. The SSPO on the illuminated rough surface is located at $59.25\,\mathrm{m} = 197.5\lambda$ away apart from the left termination. Incident angle of tapered wave is $\theta^{in} = 80^\circ$, permittivities of dry and wet soil are $\varepsilon_{dry} = 5.56 + i0.4$ and $\varepsilon_{wet} = 15.0 + i4.0$, respectively. Here the permittivity of wet soil $\varepsilon_{wet} = 15.0 + i4.0$ is typical value for a moist soil [11], and the permittivities of dry soil $\varepsilon_{dry} = 5.56 + i0.4$ contains 10% soil moisture at L band (1.43 GHz) [34]. The parameters of fractal dielectric rough surface are, fractal dimension $D = 1.3$, $M = 10$, $b = \frac{e}{2}$, $K_0 = \frac{2\pi}{33.33\lambda}$ and rms $\delta = 0.3cm = 0.01\lambda$, correlation length $l = 32.4\,\mathrm{cm} = 1.08\lambda$.

3.1. Validation of FBM/SAA for Complex Inhomogeneous Rough Surface

The normalized bistatic scattering and transmitting coefficients from both TE and TM wave are defined in [35] and [26]. The reflectivities (R) or transmittivities (T) of TE and TM waves are obtained through integrating bistatic scattering over the up-half or down-half space. In absence of absorption through the dielectric media, the unitarity condition must be satisfied for the energy conservation ($R + T = 1$), which can be used to test the numerical accuracy.

The accuracy and efficiency of FBM/SAA and FBM are verified through one surface realization, the density of unknown set $20/\lambda$, and the wet soil model is used. The convergence for both FBM

and FBM/SAA is arrived at the residual error $< 10^{-3}$. The time consuming of FBM/SAA is much effective as listed in the following Table 1. Furthermore, energy conservation ($R + T = 1$) can seen in Table 2.

Table 1. Time consuming of FBM/SAA, FBM.

	TE incidence	TM incidence
FBM	96.45(minute)	78.56(minute)
FBM/SAA	55.64(minute)	42.34(minute)

Table 2. Energy conservation of FBM, FBM/SAA.

	TE incidence			TM incidence		
	R	T	R+T	R	T	R+T
FBM	0.8912	0.1143	1.0055	0.2042	0.8012	1.0054
FBM/SAA	0.8908	0.1148	1.0056	0.2036	0.8029	1.0065

3.2. Analysis the Bistatic Scattering and Transmitting Coefficients from Dielectric Rough Soil Surface with a Conducting SSPO Partially Buried by FBM/SAA

Fifty realizations were generated to implement average calculation through Monte Carlo method in this paper.

3.2.1. Comparison of Dielectric Dry Soil Surface with and without a Conducting SSPO Partially Buried

a) Phenomena: The scattering phenomena from rough soil surface with and without conducting SSPO partially buried under both TE and TM wave incidence are given in Figs. 3 and 4, we can see that there is no obvious backscattering enhancement phenomena from soil surface with the SSPO partially buried, however, backscattering enhancement occurs at angle (-60° for TE case -65° for TM case) smaller than backscattering angle (-80°), meanwhile, the differences of backscattering coefficients (**DBSC**) are 0 dB and 29 dB for TE and TM case, respectively, and the differences of specular scattering coefficients (**DSSC**) are nearly 5 dB and 1 dB for TE and TM cases, respectively.

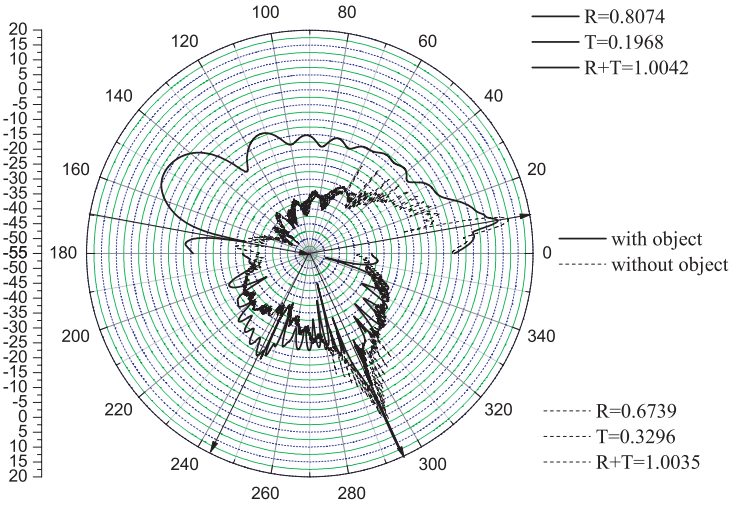

Figure 3. Bistatic scattering and transmitting coefficients from dielectric dry soil with and without a conducting SSPO (TE case).

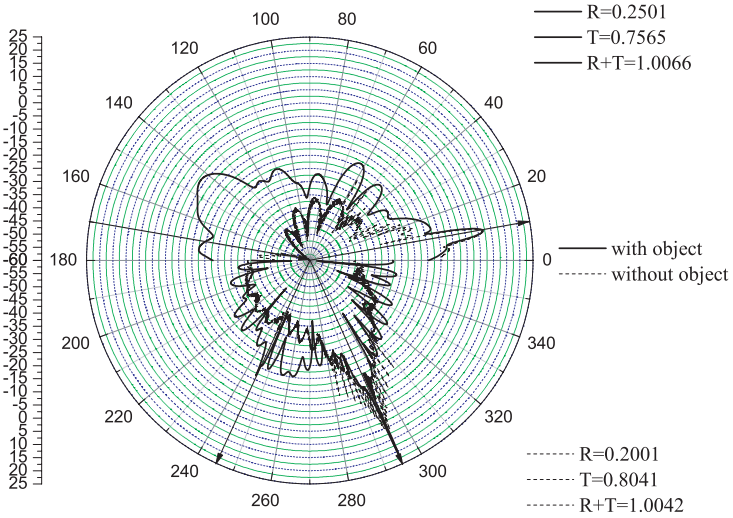

Figure 4. Bistatic scattering and transmitting coefficients from dielectric dry soil with and without a conducting SSPO (TM case).

The differences occurring to transmitting phenomena can also be seen in the same figures, it can be seen that the biggest transmitting coefficients (**TC1**) happen at 295° for both TE and TM case, the angle is nearly equal to the refraction angle 294.7 of flat dielectric surface with same permittivity. It should point out that in the 245° direction, there are large transmitting coefficients (**TC2**) from rough surface with a conducting SSPO present for both TE and TM cases, they are 16 dB and 17 dB bigger than the one from the rough surface without SSPO present for TE and TM case, respectively.

b) Explain: The **DBSC** and the backscattering enhancement occurring at a angle smaller backscattering angle is due to the conducting SSPO present. For specular scattering, considering much (or less) than half power of incident wave are scattered from (or absorbed within) the dielectric soil rough surface for TE case, on the contrary, less (or much) than half power of incident wave are scattered from (or absorbed within) the dielectric soil rough surface for TM case. When a conducting SSPO is partially buried, the SSPO will re-distribute wave scattering along its surface, make the **DSSC** of TM case smaller than the one of TE case, further, it brings large **TC2** for both TE and TM cases. However, since it size is small compared with the illuminated dielectric rough surface's length, so it will bring less variation to the **TC1** of dielectric soil rough surface.

3.2.2. Comparison of Dielectric Wet Soil Surface with and without a Conducting SSPO Partially Buried

a) Phenomena: From Figs. 5 and 6, we know that the scattering phenomena here is similar with the one of dry soil case, the two figures show that the **DBSC** from soil with and without conducting SSPO partially buried is vary large for TM case, which are 6 dB and 40 dB for TE and TM case, respectively, the **DSSC** are also nearly 5 dB and 8 dB for TE and TM cases, respectively.

For the transmitting phenomena, which is also just similar with the one of dry soil case. The two figures show that no matter if the SSPO is present or not, there also are the biggest **TC1** in refraction direction 285.0°, which is also nearly equal to the refraction angle 284.7 of flat dielectric surface with same permittivity. The differences of **TC1** between the rough surface with and without conducting SSPO partially buried are very small, it is 2 dB. It should also point out that in the 255° direction, there also is a big **TC2** from rough surface with a conducting SSPO present for both TE and TM cases, they are 16 dB and 23 dB bigger than the one from the rough surface without the conducting SSPO present for TE and TM case, respectively.

b) Explain: As we know that the scattering and transmitting

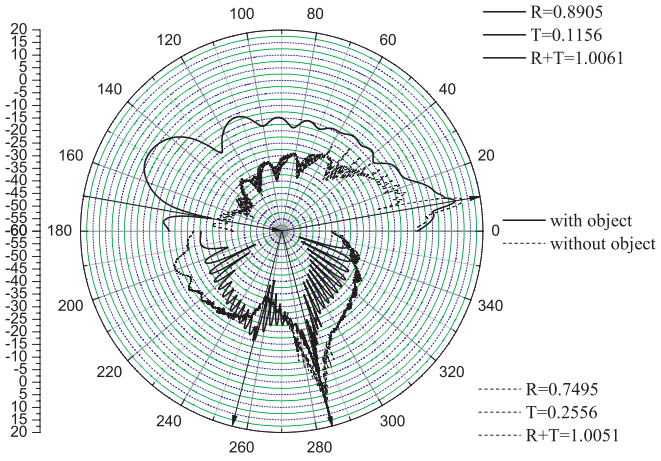

Figure 5. Bistatic scattering and transmitting coefficients from dielectric wet soil with and without a conducting SSPO (TE case).

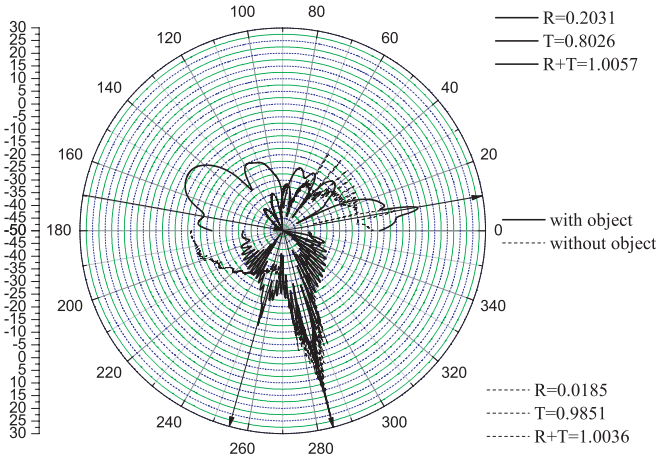

Figure 6. Bistatic scattering and transmitting coefficients from dielectric wet soil with and without a conducting SSPO (TM case).

phenomena here is similar with the one of dry soil case. Just like the phenomena, the explanation about the phenomena is also same as the one of dry soil case. Differences from dry and wet soil is brought from the permittivity of dielectric wet soil, which will be further discussed below.

3.2.3. Comparison of Dielectric Dry and Wet Soil Surface with a Conducting SSPO Partially Buried

a) Phenomena: After compared Fig. 7 with Fig. 8, we can see that a obvious backscattering enhancement phenomena from rough wet and dry soil occurring at angle smaller than backscattering angle, the two curves are superposition each other for TE case and smaller departure each other for TM case. The **DBSC** and **DSSC** of the complex rough surface for TE case are 0 dB and 1 dB. However, the **DBSC** and **DSSC** for TM case are 3 dB and 7 dB, respectively.

Transmitting phenomena within below space can also be seen in the two figures, we can see that there are two pairs of **TC1** and **TC2** for both TE and TM cases, the refraction angles of dry soil surface associated with **TC1** and **TC2** are 295° and 245° for both TE and TM cases; the refraction angles of wet soil surface associated with **TC1** and **TC2** are 285° and 255° for both TE and TM cases. The value of **TC1** and **TC2** from wet soil surface is bigger than the one from dry soil surface.

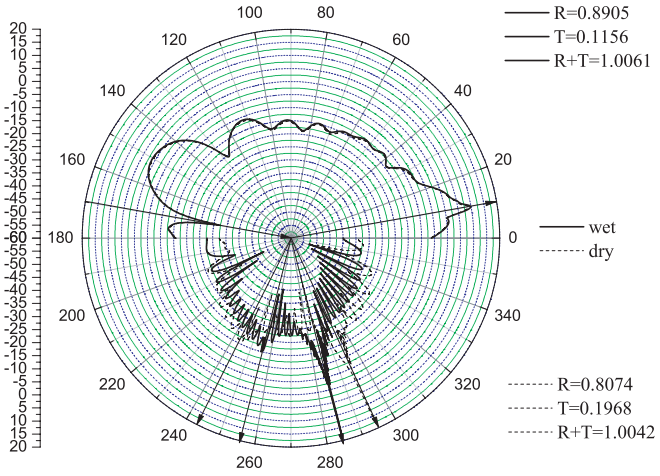

Figure 7. Difference between bistatic scattering and transmitting coefficients from dielectric wet and dry soil rough surface with a conducting SSPO soil (TE case).

b) Explanation: The backscattering enhancement occurs at different angle (−60° for TE case, −65° for TM case), both of them are smaller than backscattering angle (−80°), which is brought from the partially buried conducting SSPO, much than half power of incident wave scattered from the complex rough surface is another reason. For

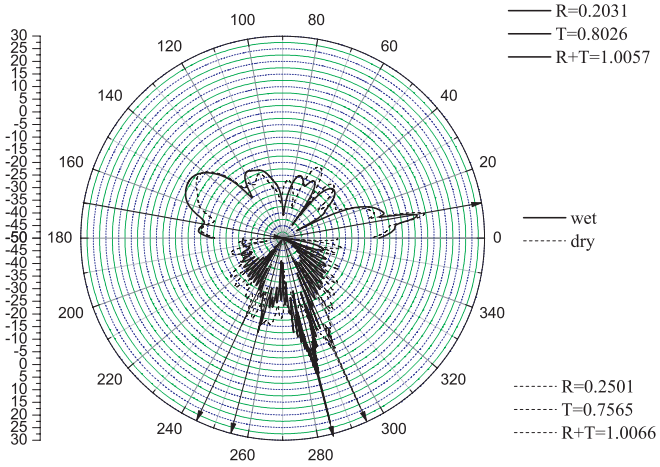

Figure 8. Difference between bistatic scattering and transmitting coefficients from dielectric wet and dry rough surface with a conducting SSPO soil (TM case).

transmitting phenomena, the different permittivities of dry and wet dielectric soil lead to different refraction angles of **TC1** and **TC2**. Since much more power of incident wave are absorbed within the wet soil surface than the dry soil surface due to bigger value of permittivity, which lead to bigger value of **TC1** and **TC2** from wet soil surface than the one from dry soil surface.

4. CONCLUSION

A hybrid approach of the FBM with SAA and Monte Carlo method for 1-D inhomogeneous complex rough surface is developed in this paper. It is applied to numerical simulation of bistatic scattering from 1-D arbitrary dielectric constant soil surface with a conducting SSPO partially buried under both the TE and TM tapered wave incidence at LGA. The energy conservation has been checked for the FBM/SAA. Numerical simulations of bistatic scattering at LGA have been discussed in this paper. the numerical results show

- No matter what kind polarization of the incident electro-magnetic wave is, backscattering coefficient from dielectric rough wet and dry soil surface with a conducting object partially buried is always large bigger than the one from dielectric rough wet and dry soil surface for TM case, but smaller for TE case.

- No matter what kind polarization of the incident electro-magnetic wave is, an obvious backscattering enhancement phenomena occurs at angle smaller 20° than backscattering angle for TE case, smaller 15° for TM case.

ACKNOWLEDGMENT

The research in this paper was supported by the Innovation Fund of Space Flight Science and Technology, and the Electromagnetic Academy at Zhejiang University.

REFERENCES

1. Holliday, D., L. L. DeRaad, and G. J. St-Cyr, "Forward-backward: A new method for computing low-grazing angle scattering," *IEEE Trans. on Anten. and Propagat.*, Vol. 44, No. 5, 722–729, 1996.
2. Kapp, D. A. and G. S. Brown, "A new numerical method for rough surface scattering calculations," *IEEE Trans. on Anten. and Propagat.*, Vol. 44, No. 5, 711–721, 1996.
3. Chou, H. T. and J. T. Johnson, "A novel acceleration algorithm for the computation of scattering, from rough surfaces with the forward-backwards method," *Radio Science*, Vol. 33, No. 5, 1277–1287, 1998.
4. Li, Z. X. and Y. Q. Jin, "Numerical simulation of bistatic scattering from a fractal rough surface using the forward-backward method," *Electromagnetics*, Vol. 22, No. 3, 191–207, 2002.
5. Holliday, D., L. L. DeRaad, and G. J. St-Cyr, "Forward-backward method for scattering from imperfect conductors," *IEEE Trans. on Anten. and Propagat.*, Vol. 46, No. 1, 101–107, 1998.
6. Chou, H. T. and J. T. Johnson, "Formulation of forward-backward method using novel spectral acceleration for the modeling of scattering from impedance rough surfaces," *IEEE Transactions on Geosicence and Remote Sensing*, Vol. 38, No. 1, 605–607, 2000.
7. Burkholder, R. J. and T. Lundin, "Forward-backward iterative physical optics algorithm for computing the RCS of openended cavities antennas and propagation," *IEEE Trans. on Anten. and Propagat.*, Vol. 53, No. 2, 793–799, 2005.
8. Zhang, P. F. and S. X. Gong, "Improvement on the forward-backward iterative physical optics algorithm applied to computing the RCS of large open-ended cavities," *Journal of Electromagnetic Wave and Application*, Vol. 21, No. 4, 457–469, 2007.

9. Jin, Y. Q. and Z. X. Li, "Bistatic scattering and transmission through a fractal rough dielectric surface using the forward and backward method with spectrum acceleration algorithm," *Journal of Electromagnetic Wave and Application*, Vol. 16, No. 4, 551–572, 2002.
10. Li, Z. X. and Y. Q. Jin, "Bistatic scattering and transmitting through a fractal rough surface with high permittivity using the physics-based two-grid method in conjunction with the forward-backward method and spectrum acceleration algorithm," *IEEE Trans. on Anten. and Propagat.*, Vol. 50, No. 9, 1323–1327, 2002.
11. Iodice, A., "Forward-backward method for scattering from dielectric rough surface," *IEEE Trans. on Anten. and Propagat.*, Vol. 50, No. 7, 901–911, 2002.
12. Iodice, A., "Scattering from natural soils modeled by dielectric fractal profile: the Forward-backward approach," *IEEE Transactions on Geoscience and Remote Sensing*, Vol. 42, No. 1, 77–85, 2004.
13. Pino, M. R., L. Landesa, J. L. Rodriguez, et al., "The generalized Forward-Backward method for analyzing the scattering from targets on ocean-like rough surfaces," *IEEE Trans. on Anten. and Propagat.*, Vol. 47, No. 6, 961–968, 1999.
14. Pino, M. R., R. J. Burkholder, F. Obelleiro, et al., "Fast generalized forward-backward method by using a spectral acceleration," *Antennas and Propagation Society International Symposium, 1999, IEEE*, Vol. 2, 1410–1413, July 11–16, 1999.
15. Wang, X., C. F. Wang, and Y. B. Gan, "Electromagnetic scattering from a circular target above or below rough surface," *Progress In Electromagnetics Research*, PIER 40, 207–227, 2003.
16. Xu, X. B. and C. M. Butler, "Current induced by TE excitation on coupled and partially buried cylinder at the interface between two media," *IEEE Trans. on Anten. and Propagat.*, Vol. 38, No. 11, 1823–1828, 1990.
17. Mallahzadeh, A. R. and M. Soleimani, "Scattering computation from the target with lossy background," *Progress In Electromagnetic Research*, PIER 57, 151–163, 2006.
18. Zhang, Y. J. and E. P. Li, "Scattering of three-dimensional chiral objects above a perfect conducting plane by hybrid finite element method," *Journal of Electromagnetic Wave and Application*, Vol. 19, No. 11, 1535–1546, 2005.
19. Chiu, T. and K. Sarabandi, "Electromagnetic scattering interaction between a dielectric cylinder and a slight rough

surface," *IEEE Trans. on Anten. and Propagat.*, Vol. 47, No. 10, 902–913, 1999.

20. Liu, P. and Y. Q. Jin, "The finite element method with domian decomposition for electromagnetic bistatic scattering from the comprehensive model of a ship on and a target above a large scale rough sea surface," *IEEE Transactions on Geoscience and Remote Sensing*, Vol. 42, No. 5, 950–956, 2004.
21. Jin, Y. Q. and Z. X. Li, "Numerical simulation of radar survellance for the ship targer and oceanic clutters in two-dimensional model," *Radio Science*, Vol. 38, No. 3, 11-1∼11-6, 2003.
22. Jin, Y. Q. and Z. X. Li, "Simulation of scattering from complex rough surface at low grazing angle using the GFBM/SAA method," *IEE J. Transactions of Fundamentals and Materials Society (A)*, Vol. 121, No. 10, 917–921, 2001.
23. Pino, M. R., R. J. Burkdolder, and F. Obelleiro, "Spectral acceleration of the generalized forward-backward method," *IEEE Trans. on Anten. and Propagat.*, Vol. 50, No. 6, 785–797, 2002.
24. Adams, R. J. and G. S. Brown, "A combined field approach to scattering from infinite elliptical cylinders using the method of ordered multiple interactions," *IEEE Trans. on Anten. and Propagat.*, Vol. 47, No. 2, 364–375, 1999.
25. Adams, R. J. and G. S. Brown, "A rapidly convergent iterative method for two-dimensional closed-body scattering problems," *Microwave and Optical Technology Letters*, Vol. 20, No. 3, 179–183, 1999.
26. Li, Z. X., "Bistatic scattering from rough dielecreic soil surface with a conducting object partially buried by using the GFBM/SAA method," *IEEE Trans. on Anten. and Propagat.*, Vol. 54, No. 7, 2072–2080, 2006.
27. Kong, J. A., *Electromagnetic Wave Theory*, 2nd edition, New York, Wiley, 1990.
28. Harrington, R. F., *Field Computation by Moment Method*, IEEE Press, New York, 1993.
29. Mandelbrot, B. B., *The Fractal Geometry of Nature*, Freeman, San Fancisco, CA, 1983.
30. Franceschetti, G., A. Iodice, M. Migliaccio, and D. Riccio, "Fractals and small perturbation scattering model," *Radio Science*, Vol. 34, No. 5, 1043–1054, 1999.
31. Jaggard, D. L. and X. Sun, "Scattering from fractally corrugated surfaces," *Journal of the Optical Society of American, A*, Vol. 7, No. 6, 1055–1062, 1990.

32. Manninen, A. T., "Multiscale surface roughness and backscattering," *Progress In Electromagnetic Research*, PIER 16, 175–203, 1997.
33. Davidson, M. W. J., T. L. Toan, F. Mattia, et al., "On the characterization of agricultural soil roughness for radar remote sensing studies," *IEEE Transactions on Geoscience and Remote Sensing*, Vol. 38, 630–640, 2000.
34. Chan, C. H., L. Tsang, and Q. Li, "Monte Carlo simulation of large-scale one-dimenrional random surface scattering at near-grazing incidence: Penetrable case," *IEEE Trans. on Anten. and Propagat.*, Vol. 46, No. 3, 142–149, 1998.
35. Sancchez-Gil, J. A. and M. Nieto-Vesperinas, "Light scattering from random rough dielectric surface," *Journal of the Optical Society of America, A*, Vol. 8, No. 8, 1270–1286, 1991.